https://doi.org/ 10.33472/AFJBS.6.5.2024.505-521

African Journal of Biological Sciences

Advancements in Nanodevice Design for Label-Free Detection of Biomolecules

Debasis Mukherjee
Department of Electronics and Communication Engineering
Brainware University
Barasat, Kolkata, West Bengal 700125, India
debasismukherjee1@gmail.com

Debarati Sarkar*
Department of Electronics and Communication Engineering
Brainware University
Barasat, Kolkata, West Bengal 700125, India
and
Department of Electronics
Vivekananda College
Thakurpukur, Kolkata, West Bengal700063, India
debarati881@gmail.com

Dr. Shashi Kant Dargar
Department of Electronics and Communication Engineering
Kalasalingam Academy of Research and Education
Tamilnadu, India 626126
drshashikant.dargar@ieee.org

Article History
Volume 6, Issue 5, Apr 2024
Received: 11 Apr 2024
Accepted: 19 Apr 2024
doi: ***10.33472/AFJBS.6.5.2024.505-521***

Abstract:

In the realm of nanotechnology, the detection of biological molecules poses both challenges and opportunities. This paper introduces a novel device structure, the CPB DM-JLTFET, designed to address complications encountered during nanodevice manufacturing, such as temperature coefficient variations and dopant concentration fluctuations. Leveraging charge plasma principles, this innovative structure incorporates an oxide substance in the etching process, resulting in an underlap zone within the nanodevice. Through label-free detection techniques reliant on the electrical characteristics of biomolecules, the CPB DM-JLTFET demonstrates superior performance attributes, including enhanced sensitivity and reduced leakage current compared to existing FET devices. A comprehensive analysis of device factors, including cavity length and thickness, reveals their significant influence on detection sensitivity. Utilizing ATLAS software for simulation, this research underscores the potential of the CPB DM-JLTFET in advancing the development of cost-efficient biomedical diagnostic tools.

Keywords: Biomolecules, TFET, transistor, semiconductor, nano

1. INTRODUCTION

Biosensors(Naresh & Lee, 2021), analytical instruments capable of detecting target molecules without invoking a reaction system, hold immense potential for high-sensitivity biomolecule detection(Malhotra et al., 2016). Contrary to conventional wisdom, the significance of biosensors amplifies with decreasing biomolecule size, especially in the realm of high-target biosensors (HTB)(Iwanaga, 2021) utilizing dielectric and charge density principles(Stobiecka et al., 2017). This study focuses on harnessing dielectric constants within a Field-Effect Transistor (FET) (Reddy & Panda, 2021)biosensing framework to achieve precise biomolecule detection. However, challenges such as temperature sensitivity, real-time analysis, and Random Dopant Fluctuations (RDF) pose significant obstacles to practical biosensor implementation(Nguyen et al., 2017). To address these challenges, meticulous consideration of surface potential, spacer length, thickness, and cavity alignment becomes imperative in sensor design.

Proposed advancements in vertical device architecture aim to mitigate Short Channel Effects (SCE)(Zanoni et al., 2024) by incorporating multiple gates(Ajay et al., 2015). The immobilization of charged biomolecules beneath the gate nanocavity alters the dielectric constant at the semiconductor-oxide interface, manifesting discernible changes in electrical specifications. Consequently, understanding the influence of ordered parameter disparities on sensitivity and device current becomes paramount. Traditional TFET fabrication processes, reliant on high process-ion and high-temperature annealing thermal budgets, encounter formidable dopant fluctuation issues, exacerbating RDF-induced current fluctuations(Kanungo et al., 2016).

To surmount these obstacles, this study employs Plasma and electrostatic technologies, with Plasma doping introducing the charge plasma doping JLTFET. The integration of a dual-gate structure, comprising distinct gate electrodes with varied work functions, enhances device performance. The JLTFET design resolves manufacturing challenges while augmenting subthreshold slope. Notably, the JLTFET gate underlay facilitates the engraving of a hollow area, enriching the cavity region for biomolecule attachment.

Moreover, the study proposes the double-gate dielectric-modulated JLTFET (DGDMJLTFET) biosensor, featuring a nanocavity space above the tunneling junction for biomolecule immobilization. Wet etching techniques are employed to create the nanocavity, albeit concerns regarding biomolecule partial filling and steric resistance necessitate thorough simulation and analysis. By evaluating drain current, ION/IOFF ratio, and subthreshold sensitivity to both neutral and charged biomolecules across various dielectric constants, this study elucidates the DGDMJLTFET's superior sensitivity and performance in biomolecule detection.

2. PROPOSED STRUCTURE

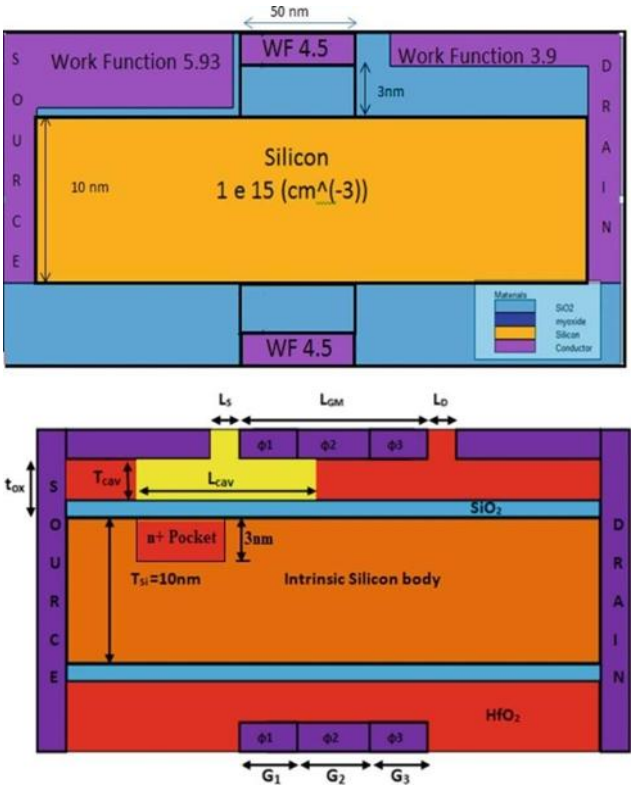

(a)

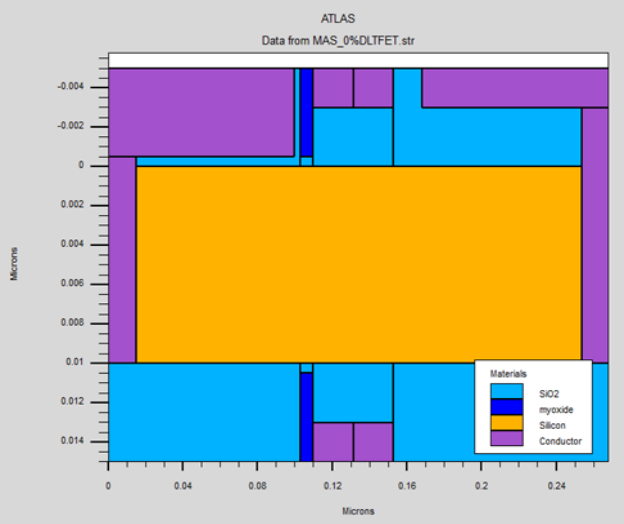

(b)

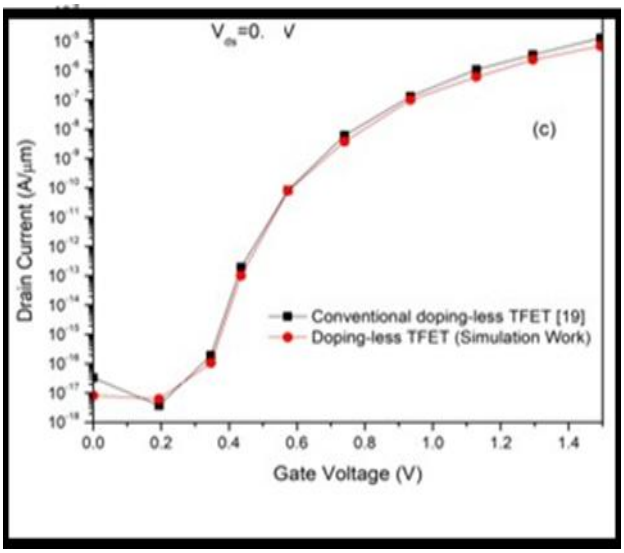

(c)

Figure1.Structures (a) TFET (b) Underlap dielectric modulated JLTFET incorporating a charge-plasma-based gate, (c) Comparison.

Figure 1 depicts the features curve for TFETs(Pown& Lakshmi, 2020) alongside the innovative CPB DM-JLTFET structure. The design incorporates specific metal work function electrodes to induce source and drain regions within an ultrathin silicon film. A block of platinum is utilized to generate holes on the source side in conjunction with an intrinsic silicon semiconductor.

Imitation include the Debye length, determined by factors. Notably, the gate overlap area and gate underlap region are critical aspects of the channel. The intrinsic one, set at approximately 1.0E+15 cm^-3, is employed for device characterization.

The opening area distance, ranging from 5 nano to 7 nm, corresponds to lengths of gates underlap. SiO2 sheet separates electrodes, while drain-gate spacers measure 15 nm in thickness and source-gate spacers 3 nm. Resultsclosely resemble those of the standard device, exceptfor the additional gate underlap area.

3. RESULTS AND DISCUSSION

In modelling the electrical properties of the device, consideration is given to the dielectric constant of the gate underlaps and overlaps. Additionally, for charged biomolecules, the fixed charge of the SiO2 interface area is accounted for.

3.1 Influence on energy bands

Fig. 2(a) and 3 depict the impact of particles. The formation of cavities within the transistor elevates the barrier, thereby reducing the likelihood of electron tunnelling and subsequently decreasing current conduction(Ghosh & Akram, 2013).

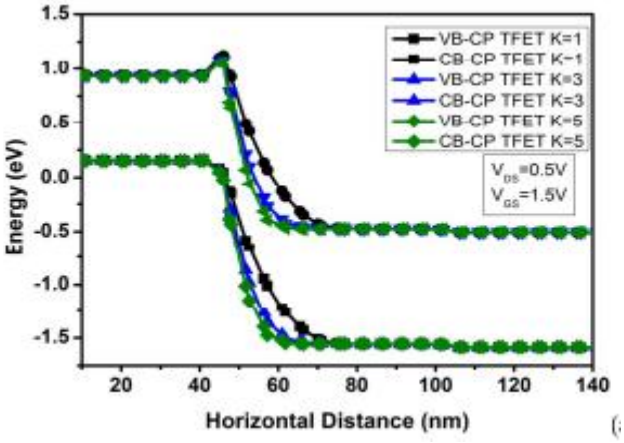

(a)

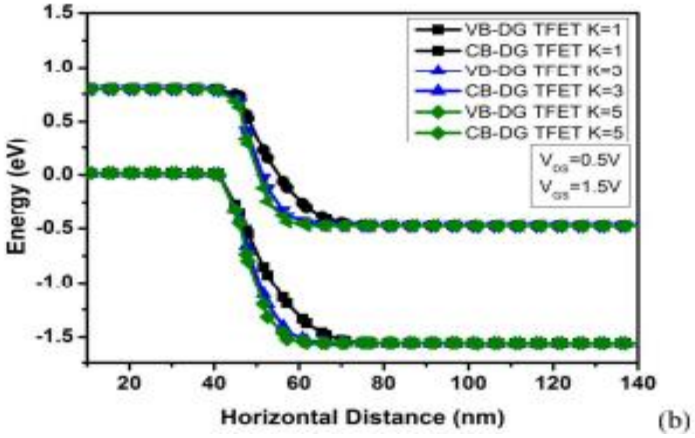

(b)

Figure 2.Alteration of conduction and valence bands due to (a) neutral biomolecules with values of K maintainedatone, three and five (b) influence of living particles with charge (Nf=–5e11 and 5e11) at Vgs=1.5V; Vds=0.5V, affecting the 5 nm cavity length.

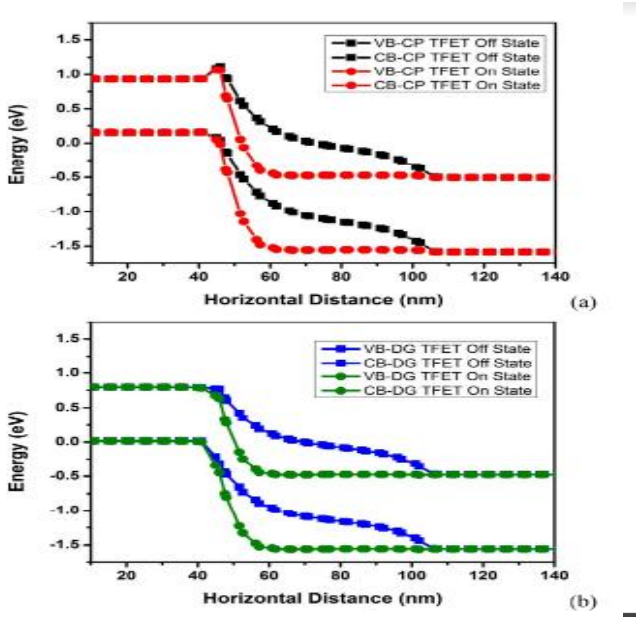

Figure 3.Variation of CV and value VB ranges for cavity lengths of 5 & 7 nm (a) K = 2 & K =10 (b) Nf=–5e11 & 5e11 with$V_{Gate\text{-}Source}$=0.5 Volt, $V_{Drain\text{-}Source}$=0 Volt.

Moreover, an increase in dielectric constant results in heightened band bending, leading to a reduction in barrier width(Narang et al., 2012). With cavity lengths set at 5 nm and 7 nm, Figure 3(c) illustrates alterations in the conduction and valence bands as cavity length varies, while increasing electron tunneling probability. Figures 2(b) and 3(b) demonstrate the significant influence of charged living particles on the device's bands. Biomolecules attached

to the cavity affect the barrier width between the source's valence band and the channel's conductive band(Chandan et al., 2018).

A result is obtained as an upsurge in opening length from 7 nano to 10 nm is approximately 0.0%.

3.2 Influence of uncharged and chargedliving biomolecules

For the variation with biomolecules present within the nanogap, leads to an increase in air's dielectric constant (K = 1).

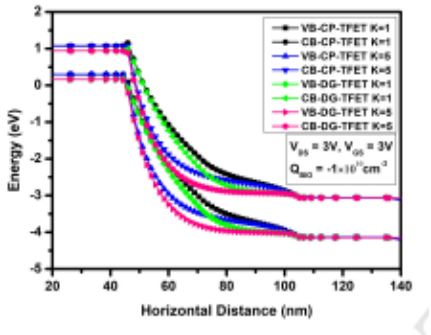

Figure 4. Surface potential variation with neutral biomolecules at a cavity length of 5, Vgs=3 V.

The filling of the cavity with biomolecules results in a significant rise in gate capacitance, rendering it an optimal sensor choice for CPB(Sant et al., 2018). However, as the dielectric constant increases, the effective capacitance decreases, impacting barrier width. Notably, immobilizing charged biomolecules in the gate underlap area induces remarkable fluctuations in surface potential(Mehrotra, 2016). For instance, when K=6 and nf=-110^10 to 110^12 cm^-2, the presence of positively charged biomolecules leads to increased surface potential. Moreover, the entry of neutral biomolecules into the cavity is facilitated.

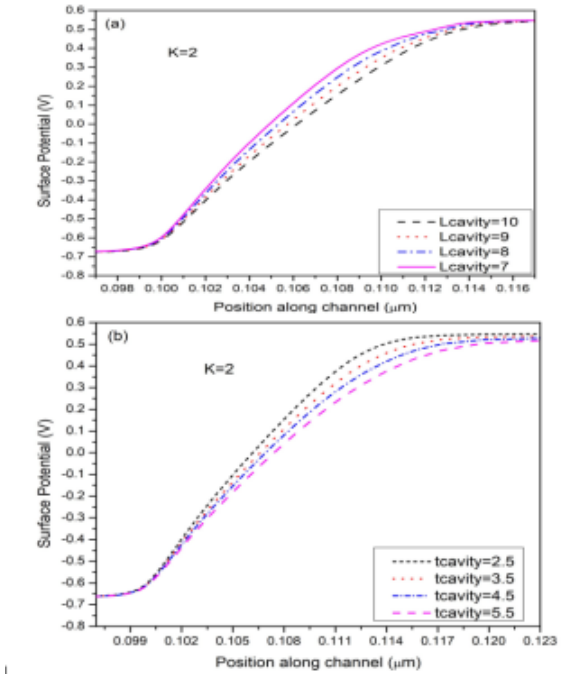

Figure 5. Surface potential variation at Vds=0 V & Vgs=0.5V.

Biomolecules with negative charges induce an elevation in flat band voltage within the overlap area, resulting in a reduction in effective gate bias(Samuel & Rao, 2022). Consequently, a decrease in surface potential occurs. Conversely, living elements with positive charge densities elicit a distinct response, as demonstrated in Figure 5(b).

Table 1.k of Different particles

Particles	K	Publication
Lysine	3.3	Yoon et al, (2020).(Yoon et al., 2020)
Arginine	3.2	Wadhwa & Raj, (2019).(Wadhwa & Raj, 2019)
Uricase	1.54	Wadhwa& Raj, (2018).(Wadhwa & Raj, 2018)
Protein	2.50	Intekhab Amin et al., (2016).(Anand et al., 2016)

The table presents dielectric constant values for select biomolecules, each with varying conductivity. Biomolecules interacting within the gate underlap area remain unutilized, with the gate underlap configuration for DM-JLFET under consideration.

3.3 Variation of Surface Potential with Cavity Length and Thickness

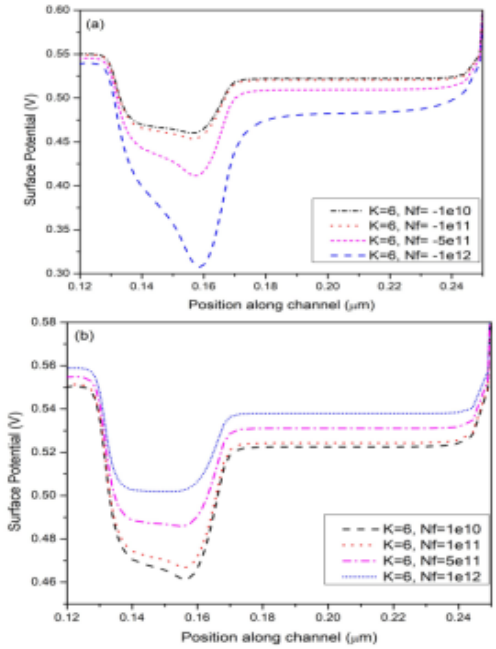

Figure 6. (a) different cavity lengths when tcavity= 2.5 nm (b) Lcavity= 5 nm.

The widening of the barrier due to cavity formation results in a decrease in surface potential. As cavity length increases, the device's surface potential diminishes, with a 7-nm-long cavity exhibiting lower surface potential than a 10-nm-long one(Ajay et al., 2013). Moreover, an increase in gate overlap area thickness leads to a drop in surface potential. As the opening escalates, the surface potential variance reduces. Notably, the maximum surface potential is achieved when the cavity is 2.5 nm thick. Fluctuations in surface potential occur at the source-channel junction due to biomolecule conjugation, particularly with a channel length set at 7 nm.

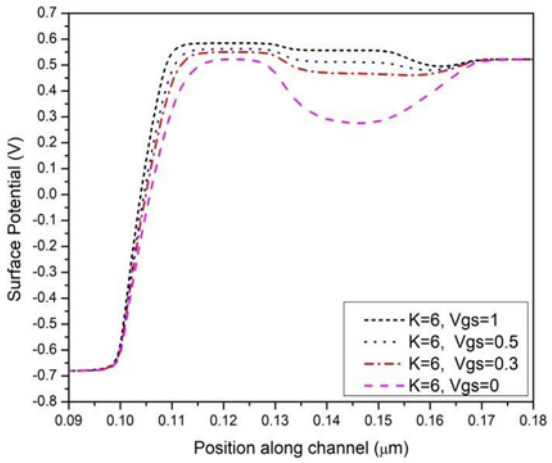

Figure 7. Surface potential variation sensitivity characteristics.

As gate bias increases, the gate-to-channel coupling weakens. However, with continued rise in gate bias, the two behaviors converge, indicating complete gate control. Approximately one million volts in surface potential change corresponds to one million volts in gate bias voltage. Comparative analyses of surface potential investigations highlight significant alterations due to biomolecule sample characteristics under suitable biasing conditions.

3.4 Surface Potential Sensitivity Variance

Biosensors' efficacy can be evaluated through their surface potential sensitivity, gauging their responsiveness to positive and negative potentials. Surface potential sensitivity is calculated using the formula: (bio-z)/z, which equals (100% bio-b) where z represents volumetric potential. When the cavity is vacant, surface potential values for z and zbio are: z = 0 and zbio = 0.

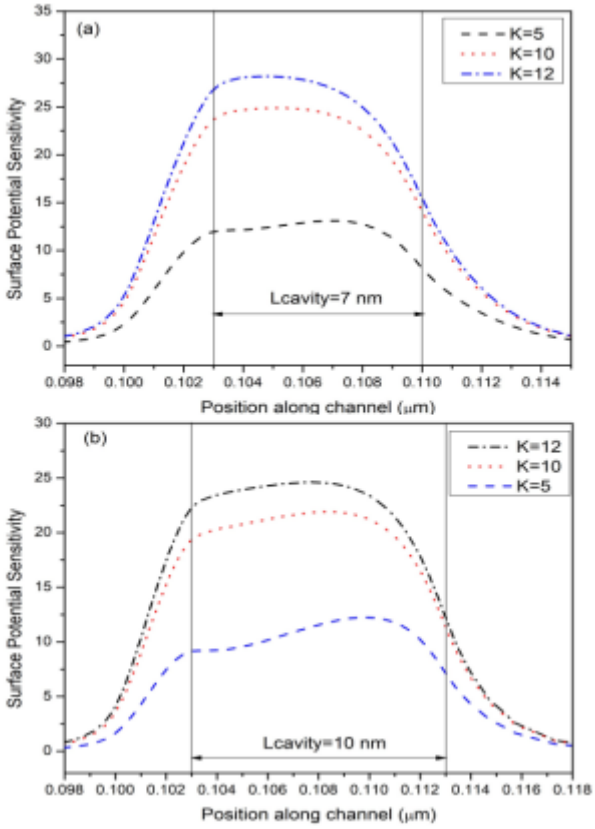

Figure 8. (a) The opening is 7 nm and (b) 10 nm.

In Figure 8, parameters are presented as a function of cavity length, utilizing a dielectric constant with Vgs and Vds equal to 0.3v and 0v, respectively (Park et al., 2012). When biomolecule concentration increases, biomolecules immobilized within the cavity enhance surface potential sensitivity concerning dielectric constant change. The CPB DM-JLTFET device's biomolecule detection capability within the cavity correlates.

The incidence of +ve living particleslessensbarrier thickness, consequently enhancing surface potential sensitivity. Conversely, the effect of charged living particles on surface potential compassion substantially upsurges with proteins that are +ve, while it diminutions with negatively charged biomolecules in the gate overlap zone. Increased charged biomolecules result in barrier band bending, further decreasing barrier width and significantly augmenting surface potential sensitivity.

3.5 Sensitivity of Ion/Ioff Ratio to Cavity Length Fluctuation

The impact varies with the opening. Ion state current begins to decrease as gate capacitance diminishes.

Table 2a. Cavity Length Change at Vgs and Vds

Cavity Length	**Vgs=1.5v, Vds=0.5v**	**Vgs=1.5v, Vds=1.5v**
	Ioff	Ion
5 nm	3.89E-18	6.08E-11
7 nm	3.91E-18	6.31E-13

Table 2b. Cavity Length Change at Vgs and Vds

Cavity Span	**1.5 VoltV$_{\text{Gate-Source}}$, 0.5 VoltV$_{\text{Drain-Source}}$**	**Vgs=1.5, Vds=1.5**
	Ioff	Ion
5 nm	3.85E-18	1.68E-10
7 nm	4.32E-18	3.19E-12

The results presented in Table III indicate the influence of neutral biomolecules, termed ion/Ioff ratio. K=1, 2, 3, 6, 10 exert different effects on the Ion/Ioff ratio of the devices. An increase in the Ion/Ioff ratio occurs as barrier width decreases. Ion/Ioff ratio serves as a determinant of the sensor's sensitivity. However, the Ion/Ioff ratio varies once the opening is 5 nm and 7 nano for the CPB DM-JLTFET device.

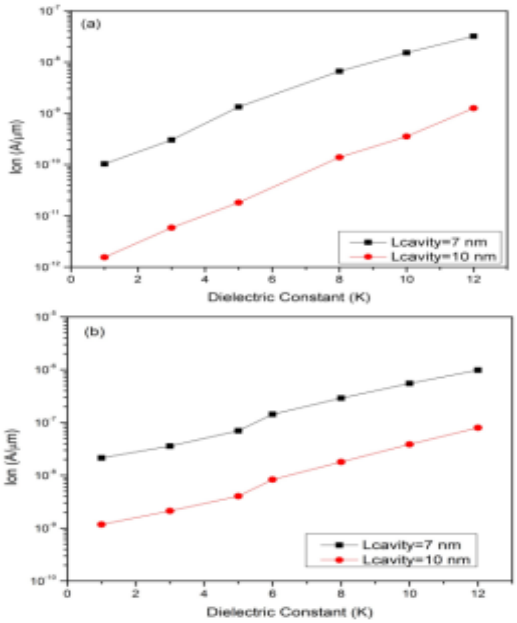

Figure 9. Plots of Ion when (a) 1.5Volt$V_{Gate\text{-}Source}$and 0.5 Volt$V_{Drain\text{-}Source}$ (b) $V_{Gate\text{-}Source}$and$V_{Drain\text{-}Source}$ 1.5Volt.

3.6 Sub-threshold slope (SS)

Another crucial parameter for examination is the sub-threshold slope (SS) Unlike thermionic emission, the SS relies on tunneling principles (Vds= 0.5v and 1.5v). As the dielectric constant increases, the value of SS begins to decrease. This indicates that the SS parameter reaches a minimum at 7 nm, compared to 10 nm. Fig. 10 illustrates the decrease in SS due to an increase in the dielectric constant.

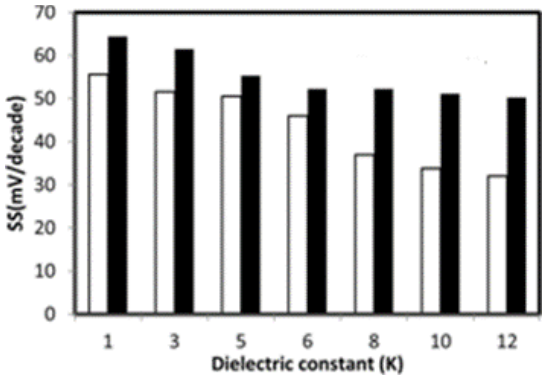

Figure 10.Ploting of SS when (a) Vgs 1.5V & Vds 0.5V (b) at Vgs&Vds 1.5V.

4. SUMMARY

The CPB DM-JLTFET structure dowries a highly effective approach for detecting immobilized biomolecules. With features like label-free detection, significant improvements in sensitivity, and a larger Ion/Ioff ratio, this device offers a cost-cutting clarification for the growth of biomedical diagnostic apparatuses. Through careful choice of cavity dimensionsadjoining the intersection of tunnelling under the right voltagesettings, maximum sensitivity is achieved. The evaluation of biomolecule effects on the electrical properties of the device reveals significantly lower leakage currents and enhanced sensitivity to charged biomolecules compared to existing FET devices, highlighting the superior performance of the CPB DM-JLTFET structure.

References:

Ajay, Narang, R., Gupta, M., & Saxena, M. (2013). Investigation of Dielectric-Modulated Double-Gate Junctionless MOSFET for detection of biomolecules. *2013 Annual IEEE India Conference, INDICON 2013*. https://doi.org/10.1109/INDCON.2013.6725863

Ajay, Narang, R., Saxena, M., & Gupta, M. (2015). Investigation of dielectric modulated (DM) double gate (DG) junctionless MOSFETs for application as a biosensors. *Superlattices and Microstructures*, *85*. https://doi.org/10.1016/j.spmi.2015.04.040

Anand, S., Amin, S. I., & Sarin, R. K. (2016). Analog performance investigation of dual electrode based doping-less tunnel FET. *Journal of Computational Electronics*, *15*(1). https://doi.org/10.1007/s10825-015-0771-4

Chandan, B. V., Nigam, K., & Sharma, D. (2018). Junctionless based dielectric modulated electrically doped tunnel FET based biosensor for label-free detection. *Micro and Nano Letters*, *13*(4). https://doi.org/10.1049/mnl.2017.0580

Ghosh, B., & Akram, M. W. (2013). Junctionless tunnel field effect transistor. *IEEE Electron Device Letters*, *34*(5). https://doi.org/10.1109/LED.2013.2253752

Iwanaga, M. (2021). High-Sensitivity High-Throughput Detection of Nucleic Acid Targets on Metasurface Fluorescence Biosensors. *Biosensors*, *11*(2). https://doi.org/10.3390/BIOS11020033

Kanungo, S., Chattopadhyay, S., Gupta, P. S., Sinha, K., & Rahaman, H. (2016). Study and Analysis of the Effects of SiGe Source and Pocket-Doped Channel on Sensing Performance of Dielectrically Modulated Tunnel FET-Based Biosensors. *IEEE Transactions on Electron Devices*, *63*(6). https://doi.org/10.1109/TED.2016.2556081

Malhotra, B. D., Kumar, S., & Pandey, C. M. (2016). Nanomaterials based biosensors for cancer biomarker detection. *Journal of Physics: Conference Series*, *704*(1). https://doi.org/10.1088/1742-6596/704/1/012011

Mehrotra, P. (2016). Biosensors and their applications - A review. In *Journal of Oral Biology and Craniofacial Research* (Vol. 6, Issue 2). https://doi.org/10.1016/j.jobcr.2015.12.002

Narang, R., Saxena, M., Gupta, R. S., & Gupta, M. (2012). Dielectric modulated tunnel field-effect transistor-a biomolecule sensor. *IEEE Electron Device Letters*, *33*(2). https://doi.org/10.1109/LED.2011.2174024

Naresh, V., & Lee, N. (2021). A review on biosensors and recent development of nanostructured materials-enabled biosensors. In *Sensors (Switzerland)* (Vol. 21, Issue 4). https://doi.org/10.3390/s21041109

Nguyen, V. T., Kwon, Y. S., & Gu, M. B. (2017). Aptamer-based environmental biosensors for small molecule contaminants. In *Current Opinion in Biotechnology* (Vol. 45). https://doi.org/10.1016/j.copbio.2016.11.020

Park, C. H., Ko, M. D., Kim, K. H., Baek, R. H., Sohn, C. W., Baek, C. K., Park, S., Deen, M. J., Jeong, Y. H., & Lee, J. S. (2012). Electrical characteristics of 20-nm junctionless Si nanowire transistors. In *Solid-State Electronics* (Vol. 73). https://doi.org/10.1016/j.sse.2011.11.032

Pown, M., & Lakshmi, B. (2020). Investigation of Radiation Hardened TFET SRAM Cell for Mitigation of Single Event Upset. *IEEE Journal of the Electron Devices Society*, *8*. https://doi.org/10.1109/JEDS.2020.3002265

Reddy, N. N., & Panda, D. K. (2021). Nanowire gate all around-TFET-based biosensor by considering ambipolar transport. *Applied Physics A: Materials Science and Processing*, *127*(9). https://doi.org/10.1007/s00339-021-04840-y

Samuel, V. R., & Rao, K. J. (2022). A review on label free biosensors. In *Biosensors and Bioelectronics: X* (Vol. 11). https://doi.org/10.1016/j.biosx.2022.100216

Sant, S., Aguirre, P., Hahn, H., Deshpande, V., Czornomaz, L., & Schenk, A. (2018). Impact of Floating Body Effect, Back-Gate Traps, and Trap-Assisted Tunneling on Scaled In_{0.53}Ga_{0.47}As Ultrathin-Body MOSFETs and Mitigation Measures. *IEEE Transactions on Electron Devices*, *65*(6), 2578–2584. https://doi.org/10.1109/TED.2018.2824021

Stobiecka, M., Jakiela, S., Chalupa, A., Bednarczyk, P., &Dworakowska, B. (2017). Mitochondria–based biosensors with piezometric and RELS transduction for potassium uptake and release investigations. *Biosensors and Bioelectronics*, *88*. https://doi.org/10.1016/j.bios.2016.07.110

Wadhwa, G., & Raj, B. (2018). Label Free Detection of Biomolecules Using Charge-Plasma-Based Gate Underlap Dielectric Modulated Junctionless TFET. *Journal of Electronic Materials*, *47*(8). https://doi.org/10.1007/s11664-018-6343-1

Wadhwa, G., & Raj, B. (2019). Design, Simulation and Performance Analysis of JLTFET Biosensor for High Sensitivity. *IEEE Transactions on Nanotechnology*, *18*. https://doi.org/10.1109/TNANO.2019.2918192

Yoon, J., Shin, M., Lee, T., & Choi, J. W. (2020). Highly sensitive biosensors based on biomolecules and functional nanomaterials depending on the types of nanomaterials: A perspective review. In *Materials* (Vol. 13, Issue 2). https://doi.org/10.3390/ma13020299

Zanoni, E., De Santi, C., Gao, Z., Buffolo, M., Fornasier, M., Saro, M., De Pieri, F., Rampazzo, F., Meneghesso, G., Meneghini, M., Zagni, N., Chini, A., &Verzellesi, G. (2024). Microwave and Millimeter-Wave GaN HEMTs: Impact of Epitaxial Structure

on Short-Channel Effects, Electron Trapping, and Reliability. *IEEE Transactions on Electron Devices*, *71*(3). https://doi.org/10.1109/TED.2023.3318564